(A New Proposal to Jefferson Lab PAC27)

Initial State Helicity Correlation in Wide Angle Compton Scattering

P. Bosted, J. P. Chen, E. Chudakov, K. DeJager, R. Ent, R. Feuerbach, J. Gomez, D. Gaskell, O. Hansen, D. W. Higinbotham, M. Jones, J. LeRose, D. Mack, R. Michaels, S. Nanda, B. Reitz, A. Saha, S. Wood, B. Wojtsekhowski (spokesperson)
Thomas Jefferson National Accelerator Facility, Newport News, VA 23606

G. Cates, D. Crabb, D. Day (spokesperson), R. Lindgren, N. Liyanage, V. Nelyubin, O. Rondon, K. Slifer, L.C. Smith, S. Tajima
University of Virginia, Charlottesville, VA 22904

R. Asaturyan, K. Egiyan, V. Mamyan, H. Mkrtchyan, T. Navasardyan, A. Shahinyan, V. Tadevosyan, H. Voskanyan
Yerevan Physics Institute, Yerevan, Armenia

D. Nikolenko, I. Rachek, Yu. Shestakov
Budker Institute, Novosibirsk, Russia

F. Butaru, A. Lukhanin, Z.-E. Meziani, B. Sawatsky, P. Solvignon, H. Yao
Temple University, Philadelphia, PA 19122

P. Markowitz
Florida International University, Miami, FL 33199

M. Khandaker, V. Punjabi, F. Wesselmann
Norfolk State University, Norfolk, VA 23504

B. Crowe, B. Vlahovic
North Carolina Central University, Durham, NC 03824

C. Glashausser, R. Gilman, X. Jiang, G. Kumbartzki, R. Ransome
Rutgers, The State University of New Jersey, Piscataway, NJ 08854

E. Piasetzky, G. Ron
Tel Aviv University, Israel

C. Perdrisat, L. Pentchev
College of William and Mary, Williamsburg, VA 23185

C. Hyde-Wright, A. Radyushkin,
Old Dominion University

D. Margaziotis
California State University Los Angeles, Los Angeles, CA 90032

December 6, 2004

Contents

Abstract

We propose an experiment to measure the initial state helicity correlation asymmetry A_{LL} in Real Compton Scattering (RCS) by scattering longitudinally polarized photons from a longitudinally polarized proton target. A measurement will be done at the invariant energy s= 9 (GeV/c)^2 for two scattering angles, $\theta_\gamma^{cm} = 70^\circ$ and 140°.

The recent JLab RCS experiment, E99-114, demonstrated the experimental feasibility of a mixed photon-electron beam for Compton scattering and also produced a remarkable result. Namely, at s = 7 (GeV/c)^2 and $\theta_\gamma^{cm} = 120^\circ$, the longitudinal polarization transfer observable K_{LL} is in agreement with a handbag description of the process in which the photons interact with a single quark, consistent with a prediction made by P. Kroll *et al.* within the GPD framework. The E99-114 results are, in fact, then inconsistent with the pQCD mechanism involving three active quarks.

The applicability of QCD (in the JLab energy range) to exclusive reactions is a subject of great interest and any opportunity to test unambiguously its prediction should be taken. Recent calculations by G. A. Miller in a constituent quark model reproduced the K_{LL} experimental result but revealed a large disagreement with the GPD prediction for A_{LL}. It is but one of the goals of our proposal to test this prediction which could force a modification of our understanding of the high-t photo-induced processes like RCS, pion photoproduction, and deuteron photo–disintegration.

The experiment utilizes an untagged bremsstrahlung photon beam and the UVA polarized target. The scattered photon is detected in the BigCal photon spectrometer, currently under construction by the GEP-III collaboration. The coincident recoil proton is detected in the Hall C magnetic spectrometer HMS. With 506 hours of beam time, the polarization observable A_{LL} will be measured to a statistical accuracy of better than $\pm$0.1.

This measurement will significantly increase our experimental confidence in the application of the GPD approach to reactions induced by real photons which play a major role in nucleon structure physics in the JLab energy range.

1 Introduction

Significant progress has been made over the last decade in our understanding of exclusive reactions in the hard scattering regime. This progress had been made possible (in part) by data from Jefferson Lab on elastic electron scattering and Compton scattering from the proton and by a significant and increasingly sophisticated theoretical effort to exploit the richness of exclusive reactions at moderate momentum transfers.

The observation of scaling in Deep Inelastic Scattering (DIS) at relatively low momentum transfers, successfully understood within the framework of pQCD, suggested that the same interpretation would be fruitful when applied to exclusive reactions: elastic electron scattering, photo- and electro-production of mesons, and Compton scattering. This prospect was further supported by the fact that constituent counting rules [1, 2], which naturally govern reactions that conform to the pQCD picture, could describe certain exclusive reactions.

There is little doubt that the pQCD mechanism dominates at high energies. What has been lacking is a general agreement as to how high the energy must be for pQCD to be completely applicable. The argument on this point is driven by more than a difference of (theoretical) opinion. The unavoidable fact is that cross sections calculated in a pQCD framework have invariably been low when compared to data, sometimes by an order of magnitude or more.

Results of two experiments at Jefferson Lab on the proton contradict the predictions of pQCD: the recoil polarization measurements of G_E^p E93-027 and E99-007, and the Real Compton Scattering (RCS) experiment E99-114. The G_E^p measurements[3, 4] found that the ratio of F_2 and F_1, scaled by Q^2 demands a revision of one of the precepts of pQCD, namely hadron helicity conservation. Preliminary results from the RCS measurement[5] are that the longitudinal polarization transfer K_{LL} is large and positive, also contrary to the pQCD predictions which find $K_{LL}$to be small and negative. These two experiments provide a compelling argument that pQCD should not be applied to exclusive processes at energy scales of 5-10 GeV.

Fortunately, an alternate theoretical framework exists [6, 7, 8] for the interpretation of exclusive scattering at intermediate energies. This alternative approach asserts the dominance of the handbag diagram in which the reaction amplitude factorizes into a subprocess involving a hard interaction with a *single quark*. The coupling of the struck quark to the spectator system is described by the Generalized Parton Distributions (GPD's) [9, 10]. Since the GPD's are independent of the particular hard scattering reaction, the formalism leads to a unified description of hard exclusive reactions. Moreover, the relationship between GPD's and the normal parton distribution functions provides a natural framework for relating inclusive and exclusive reactions.

The Real Compton Scattering (RCS) experiment E99-114 produced an especially remarkable result; not only was the measurement of K_{LL} inconsistent with pQCD, it was found that the longitudinal polarization is nearly as large as that expected for scattering from a free

quark! The various theoretical efforts made to apply the handbag approach to wide angle compton scattering (WACS) have produced predictions for its polarization observables including K_{LL} and A_{LL} [8, 11]. We must emphasize that the results of E99-114 are at a single kinematic point (Experiment E03-003 [12] will extend these measurements.) of a single observable. It is essential to verify the dominance of the handbag mechanism in other observables such as A_{LL}. In a recent development, a calculation of Miller suggests that a measurement of A_{LL} in WACS would be a test of perturbative chiral symmetry and of the mass of the quarks participating in the hard scattering.

We therefore propose a measurement of the polarization observable A_{LL}in Compton scattering at an incident energy of 4.3 GeV.

The proposal is organized as follows. In Section 2 we describe in more detail the handbag formalism and the predictions for RCS, some results from E99-114, and a summary of the physics goals of the proposed experiment. In Section 3 we describe the experimental approach and both the standard and the specialized equipment. In subsequent sections, we present our proposed measurements (Sec. 4), our expected results and beam time request (Sec. 5), and the technical considerations related to the equipment and the experiment schedule (Sec. 6). The collaboration commitment and experience is presented in Section 7. Finally, the proposal is summarized in Section 8.

2 Physics Motivation

2.1 Overview

In view of the remarks in the Introduction, we consider several interesting questions that motivates us to explore further the measurement of polarization observables in RCS at JLab:

1. What is the nature of quark which absorbs and emits photons in the RCS process in the wide angle regime? Is it a constituent or a current quark?

2. If the GPD approach is correct, is it indeed true that the RCS reaction proceeds through the interaction of photons with a single quark?

3. What are the constraints on the GPD integrals imposed from the proposed measurement of the A_{LL} observable.

In order to present a framework for addressing these issues, we next discuss the three reaction mechanisms: pQCD, the handbag mechanism in the GPD conceptualization, and the handbag mechanism in the constituent quark model.

2.2 pQCD Mechanism

The traditional framework for the interpretation of hard exclusive reactions in the asymptotic regime is perturbative QCD (pQCD) [13, 14]. The onset of scaling in Deep Inelastic Scattering (DIS) at the relative low scale of $Q^2 \sim 1$–2 $(\mathrm{GeV/c})^2$, gives rise to the expectation that pQCD might also be applicable to exclusive processes in the range of a few $(\mathrm{GeV}/c)^2$. pQCD confronts RCS [15, 16, 17] as shown in Fig. 2.2, where it is seen that the three valence quarks are active participants in the hard subprocess, which is mediated by the exchange of two hard gluons. The soft physics is contained in the valence quark distribution amplitudes. The pQCD mechanism leads naturally to the constituent counting rules for exclusive processes:

$$\frac{d\sigma}{dt} = \frac{f(\theta_{cm})}{s^n}, \tag{1}$$

where n is related to the number of active constituents in the reaction [1, 2]. Indeed, the observation that many exclusive reactions, such as elastic electron scattering, pion photoproduction, and RCS, approximately obey Eq. 1 has led to the belief that the pQCD mechanism dominates at experimentally accessible energies. There seems to be little theoretical disagreement that the pQCD mechanism dominates at sufficiently high energies [13]; however, there is no consensus on how high is "sufficiently high." Despite the observed scaling, absolute cross sections calculated using the pQCD framework are very often low compared to existing

experimental data, sometimes by more than an order of magnitude. Moreover, several recent JLab experiments that measure polarization observables also disagree with the predictions of pQCD. In the G_E^p experiment [3, 4] the slow falloff of the Pauli form factor $F_2(Q^2)$ up to Q^2 of 5.6 $(\mathrm{GeV}/c)^2$ provides direct evidence that hadron helicity is not conserved, contrary to predictions of pQCD. Similar findings were made in the π^0 photoproduction experiment [18], where both the non-zero transverse and normal components of polarization of the recoil proton are indicative of hadron helicity-flip, which is again contrary to the predictions of pQCD. Finally, in the recently completed RCS experiment, E99-114, the longitudinal polarization transfer K_{LL} (which will be defined precisely below) shows a value which is large and positive, contrary to the pQCD prediction which is small and negative [17]. For all these reasons, it can be argued that pQCD is not the correct mechanism for interpreting exclusive reactions at currently accessible energies and instead we should seek a description in terms of the handbag mechanism.

pQCD calculations predict that A_{LL}=K_{LL}, so a measurement of A_{LL} in combination with already obtained result for K_{LL} could provide an additional test of pQCD applicability in the JLab energy regime.

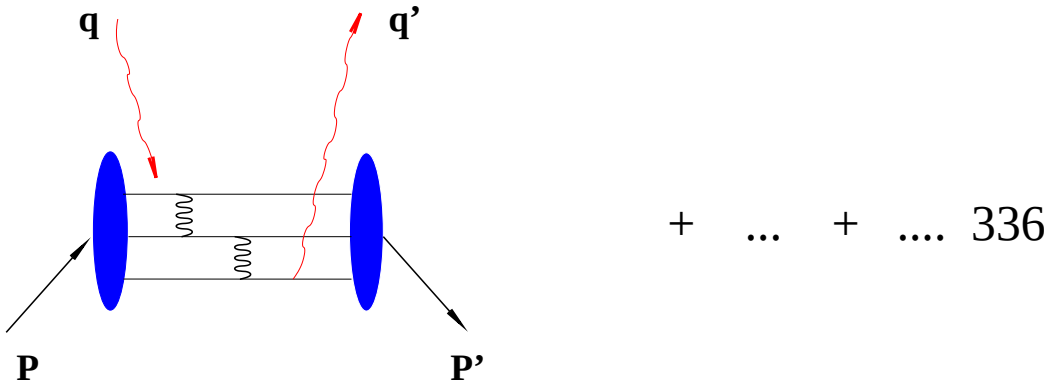

Figure 1: Two gluon exchange pQCD diagram for RCS.

2.3 Handbag Mechanism

The handbag mechanism offers new possibilities for the interpretation of hard exclusive reactions. For example, it provides the framework for the interpretation of deep exclusive reactions, which are reactions initiated by a high-Q^2 virtual photon. The application of the formalism to RCS (see Fig. 2) was initially worked out to leading order (LO) by Radyushkin [6] and subsequently by Diehl *et al.*[7]. More recently next-to-leading-order (NLO) contributions have been worked out by Huang *et al.*[8]. The corresponding diagram for elastic

electron scattering is similar to Fig. 2, except that there is only one external virtual photon rather than two real photons. In the handbag approach, the hard physics is contained in the scattering from a single active quark and is calculable using pQCD and QED: it is just Compton scattering from a structureless spin-1/2 particle.

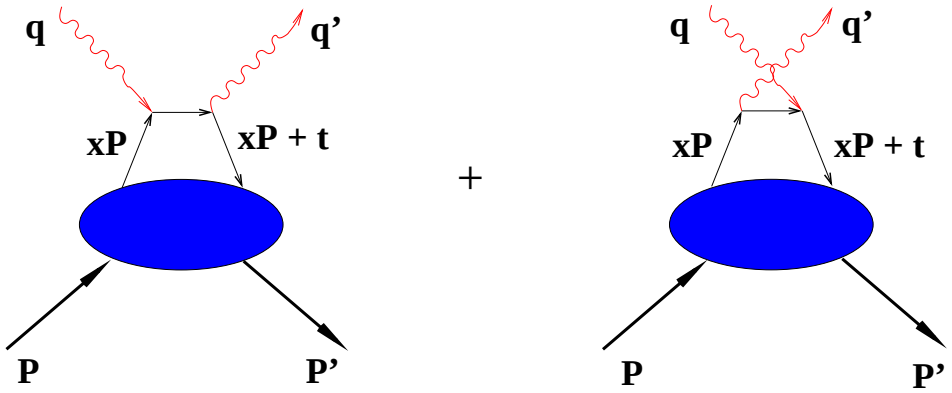

Figure 2: The handbag diagram for RCS.

The soft physics is contained in the wave function describing how the active quark couples to the proton. This coupling is described in terms of GPD's. The GPD's have been the subject of intense experimental and theoretical activity in recent years [9, 10]. They represent "superstructures" of the proton, from which are derived other measurable structure functions, such as parton distribution functions (PDF) and form factors (F_1 and F_2). To NLO, only three of the four GPD's contribute to the RCS process: $H(x,\xi=0,t)$, $\hat{H}(x,\xi=0,t)$, and $E(x,\xi=0,t)$. Since the photons are both real, the skewness parameter ξ is zero, reflecting the fact that the momentum absorbed by the struck quark is purely transverse. In the handbag formalism, the RCS observables are new form factors of the proton that are x^{-1}-moments of the GPD's:

$$
\begin{aligned}
R_{_V}(t) &= \sum_a e_a^2 \int_{-1}^{1} \frac{dx}{x} H^a(x,0,t), \\
R_{_A}(t) &= \sum_a e_a^2 \int_{-1}^{1} \frac{dx}{x} \,\mathrm{sign}(x)\, \hat{H}^a(x,0,t), \\
R_{_T}(t) &= \sum_a e_a^2 \int_{-1}^{1} \frac{dx}{x} E^a(x,0,t),
\end{aligned}
$$

where e_a is the charge of the active quark and the three form factors are, respectively, the vector, axial vector, and tensor form factors. The corresponding form factors for elastic electron or neutrino scattering are given by the first (x^0) moments of the same GPD's:

$$
\begin{aligned}
F_{_1}(t) &= \sum_a e_a \int_{-1}^{1} dx\, H^a(x,0,t), \\
G_{_A}(t) &= \sum_a \int_{-1}^{1} dx\, \mathrm{sign}(x)\, \hat{H}^a(x,0,t), \\
F_{_2}(t) &= \sum_a e_a \int_{-1}^{1} dx\, E^a(x,0,t),
\end{aligned}
$$

where the three quantities are, respectively, the Dirac, axial, and Pauli form factors. On the other hand, the $t = 0$ limit of the GPD's produce the PDF's:

$$
\begin{aligned}
H^a(x,0,0) &= q^a(x), \\
\hat{H}^a(x,0,0) &= \Delta q^a(x) \\
E^a(x,0,0) &= 2\frac{J^a(x)}{x} - q^a(x),
\end{aligned} \tag{2}
$$

where J^a is the total angular momentum of a quark of flavor a and is not directly measurable in DIS.

In the handbag factorization scheme, the RCS helicity amplitudes are related to the form factors by

$$
\begin{aligned}
M_{\mu'+,\mu+}(s,t) &= 2\pi\alpha_{em}\left[T_{\mu'+,\mu+}(s,t)(R_{_V}(t) + R_{_A}(t)) + T_{\mu'-,\mu-}(s,t)(R_{_V}(t) - R_{_A}(t))\right], \\
M_{\mu'-,\mu+}(s,t) &= 2\pi\alpha_{em}\frac{\sqrt{-t}}{m}\left[T_{\mu'+,\mu+}(s,t) + T_{\mu'-,\mu-}(s,t)\right] R_{_T}(t),
\end{aligned}
$$

where μ, μ' denote the helicity of the incoming and outgoing photons, respectively. The signs on M and T refer to the helicities of the proton and active quark, respectively. This structure of the helicity amplitudes leads to a simple interpretation of the RCS form factors: $R_{_V} \pm R_{_A}$ is the response of the proton to the emission and reabsorption of quarks with helicity in the same/opposite direction of the proton helicity, and $R_{_T}$ is directly related to the proton helicity-flip amplitude [8]. These equations leads to expressions relating RCS observables to the form factors.

The most important of these experimentally are the spin-averaged cross section and the recoil polarization observables. The spin-averaged cross section factorizes into a simple product of the Klein-Nishina (KN) cross section describing the hard scattering from a single quark, and a sum of form factors depending only on t [6, 7]:

$$
\frac{d\sigma/dt}{d\sigma_{_{\rm KN}}/dt} = f_{_V}\left[R_{_V}^2(t) + \frac{-t}{4m^2}R_{_T}^2(t)\right] + (1 - f_{_V})R_{_A}^2(t)\,, \tag{3}
$$

For the the interesting region of large $p_\perp$, the kinematic factor $f_{_V}$ is always close to 1. Consequently the unpolarized cross sections are largely insensitive to $R_{_A}$, and the left-hand-side of Eq. 3 is nearly s-independent at fixed t. The recent calculations to NLO, which take into account both photon and proton helicity-flip amplitudes, do not change this prediction in any appreciable way [8]. One of the primary goals of E99-114 was to test this relationship as well as to determine the vector form factor $R_{_V}$.

The longitudinal and transverse polarization transfer observables, $K_{_{LL}}$ and $K_{_{LS}}$, respectively, are defined by

$$K_{_{LL}}\frac{d\sigma}{dt} \equiv \frac{1}{2}\left[\frac{d\sigma(\uparrow\downarrow)}{dt} - \frac{d\sigma(\uparrow\downarrow)}{dt}\right] \qquad K_{_{LS}}\frac{d\sigma}{dt} \equiv \frac{1}{2}\left[\frac{d\sigma(\uparrow\rightarrow)}{dt} - \frac{d\sigma(\downarrow\rightarrow)}{dt}\right] \tag{4}$$

where the first arrow refers to the incident photon helicity and the second to the recoil proton helicity ($\uparrow$) or transverse polarization ($\rightarrow$).

With definitions of two additional parameters

$$\beta = \frac{2m}{\sqrt{s}}\frac{\sqrt{-t}}{\sqrt{s}+\sqrt{-u}} \qquad \kappa(t) = \frac{\sqrt{-t}}{2m}\frac{R_{_T}(t)}{R_{_V}(t)}\,, \tag{5}$$

the three polarization observables are approximately related to the form factors by the expressions [7, 8]

$$K_{_{LL}} \approx K_{_{LL}}^{\rm KN}\frac{R_{_A}(t)}{R_{_V}(t)}\frac{1-\beta\kappa(t)}{1+\kappa^2(t)} \qquad \frac{K_{_{LS}}}{K_{_{LL}}} \approx \kappa(t)\frac{1+\beta\kappa^{-1}(t)}{1-\beta\kappa(t)} \qquad P_{_N} \approx 0\,, \tag{6}$$

where $K_{_{LL}}^{\rm KN}$ is the longitudinal asymmetry for a structureless Dirac particle. These formulas do not include small gluonic corrections, which are discussed in Ref. [8].

The expressions above show that measurements of $K_{_{LL}}$ and $K_{_{LS}}$, when combined with measurements of $d\sigma/dt$ (*i.e.* from E99-114), allow determinations of all three form factors. They also show that two very important pieces of information follow directly from the spin asymmetries: $K_{_{LL}}$ and $K_{_{LS}}$ / $K_{_{LL}}$, which are directly related to the form factor ratios $R_{_A}/R_{_V}$ and $R_{_T}/R_{_V}$, respectively.

In the GPD approach of Ref. [8], the initial state helicity correlation parameter, $A_{_{LL}}$, equals $K_{_{LL}}$ so all the predicted relationships between $A_{_{LL}}$ and the RCS form factors are the same as shown above for $K_{_{LL}}$.

From the relationships connecting the RCS form factors to PDF's, Eq. 2, the ratio $R_{_A}/R_{_V}$ is related to $\Delta q^a(x)/q^s(x)$. For RCS, the e_a^2-weighting of the quark flavors means that u quarks will dominate the reaction. Moreover, at moderate-to-high $-t$, the contributions to the form-factor integral are concentrated at moderate-to-high x, where the valence quarks dominate. Therefore, the $A_{_{LL}}$ asymmetry contains direct information on $\Delta u(x)/u(x)$ in the

valence region. We propose to investigate this in the present experiment, up to $-t = 6.4$ $(\mathrm{GeV}/c)^2$.

Obtaining this kind of information is one of the key physics elements justifying the 12 GeV upgrade of JLab. From the correspondence between RCS and electron scattering form factors, there is expected to be a close relationship between $R_{_T}/R_{_V}$ and F_2/F_1 [8]. The measurements of G_E^p at JLab [3, 4] have shown that F_2/F_1 falls as $1/\sqrt{-t}$ rather than as $1/t$, the latter being predicted by pQCD. It will be an important check on the theoretical interpretation of $F_{_2}/F_{_1}$ to see if $R_{_T}/R_{_V}$ behaves in a similar way.

2.4 Constituent quark model for RCS

The constituent quark model developed by G. A. Miller [11] addresses the question of what is the dominant reaction mechanism that allows the proton to accommodate the large momentum transfer in exclusive reactions like elastic electron and photon scattering. This model has been successful in describing the electromagnetic nucleon form factors [19]. Unlike the handbag calculations within the GPD approach [7, 8], Miller's model does not neglect quark and hadron helicity flip. The model starts with a wave function for three relativistic constituent quarks:

$$\Psi(p_i) = u(p_1)u(p_2)u(p_3)\psi(p_1, p_2, p_3),$$

where p_i represents space, spin, and isospin indices. It evaluates the wave function in the light cone variables and the calculations are relativistic. They obey gauge invariance, parity conservation, and time reversal invariance. They include quark mass effects and proton helicity flip. Due to lower components of Dirac spinors, where the quark spin is opposite to that of the proton, quark orbital angular momentum appears. The resulting predictions for the polarization observables $A_{_{LL}}$ and $K_{_{LL}}$ and the cross section are shown in Fig. 3 and Fig. 4, together with data from the E99-114 experiment. The most striking consequence of Miller's results is a big difference between $A_{_{LL}}$ and $K_{_{LL}}$ at large scattering angles, which we can test experimentally.

2.5 Polarization in QED Compton process

It is instructive to evaluate polarization effects in the QED process $e\gamma \to e\gamma$. The Klein-Nishina process is an example that is fully calculable and which plays a major role in RCS, when the handbag diagram dominates. It is useful to evaluate polarization observables for different ratios of the electron mass to the photon energy.

Polarization observables in QED are given in invariant variables as [20] :

$$A_{_{LL}}^{KN} = \left[-\tfrac{s-m^2}{u-m^2} + \tfrac{u-m^2}{s-m^2} - \tfrac{2m^2t^2(s-u)}{(s-m^2)^2(u-m^2)^2}\right] / \left[-\tfrac{s-m^2}{u-m^2} - \tfrac{u-m^2}{s-m^2} + \tfrac{4m^2t(m^4-su)}{(s-m^2)^2(u-m^2)^2}\right]$$

$$K_{_{LL}}^{KN} = \left[-\tfrac{s-m^2}{u-m^2} + \tfrac{u-m^2}{s-m^2} - \tfrac{4m^2t^2(m^4-su)}{(s-m^2)^3(u-m^2)^2}\right] / \left[-\tfrac{s-m^2}{u-m^2} - \tfrac{u-m^2}{s-m^2} + \tfrac{4m^2t(m^4-su)}{(s-m^2)^2(u-m^2)^2}\right]$$

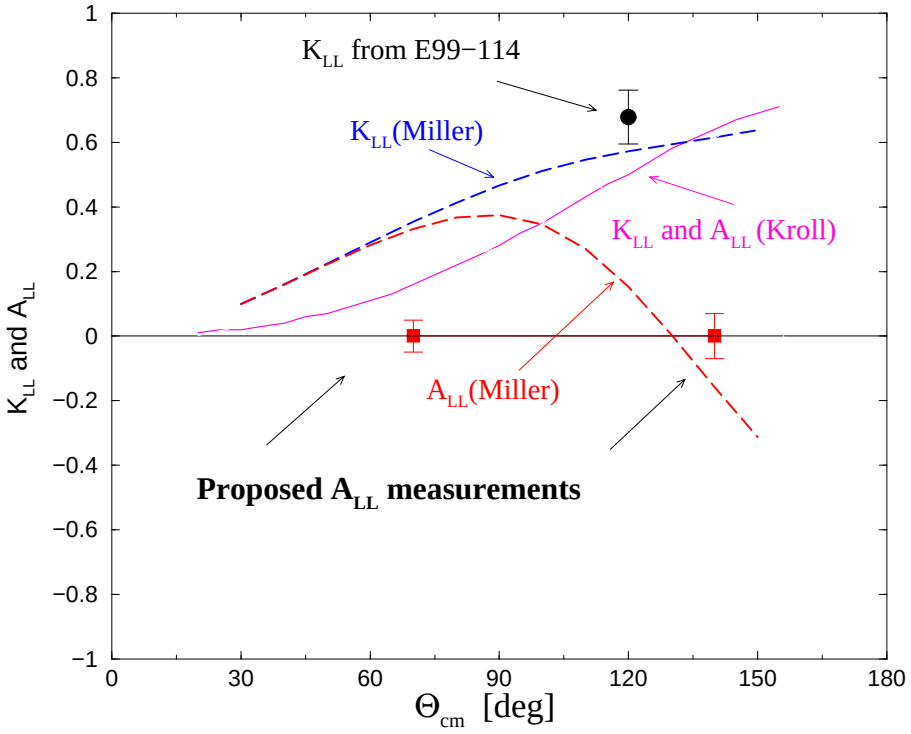

Figure 3: Predictions for A_{LL} in GPD approach [8] and CQM [11].

Fig. 5 shows the A_{LL}^{KN} and K_{LL}^{KN} for different energies of the incident photon. At low t/s and for $m/E_\gamma << 1$ the difference between K_{LL} and A_{LL} disappears. At $\theta_{lab} = \pi/2$ the observable A_{LL}=0. In the limit $m/E_\gamma \to 0$ A_{LL}=K_{LL} for all values of θ_γ not equal to 180°. At $\theta_\gamma = 180°$ the value of $A_{LL} \approx -K_{LL}$. When $m/E_\gamma \sim 1/10$ and $\theta_{lab} \approx 90°$ the difference is about 0.7.

2.6 Additional Remarks

It is important to realize that the issues posed at the start of this section are not limited to the RCS reaction. Indeed, they are questions that need to be addressed by all studies of the proton using exclusive reactions in the hard scattering regime. The old paradigm for addressing these questions was the pQCD mechanism and the distribution amplitudes. It is quite likely that the new paradigm will be the handbag mechanism and GPD's. In any case, the reaction mechanism needs to be tested, not only over a wide range of kinematic variables but also over a wide range of different reactions. Of these, RCS offers the best possibility to test the mechanism free of complications from additional hadrons. The CQM was quite successful in its description of many observables of the hadronic structure and generates a

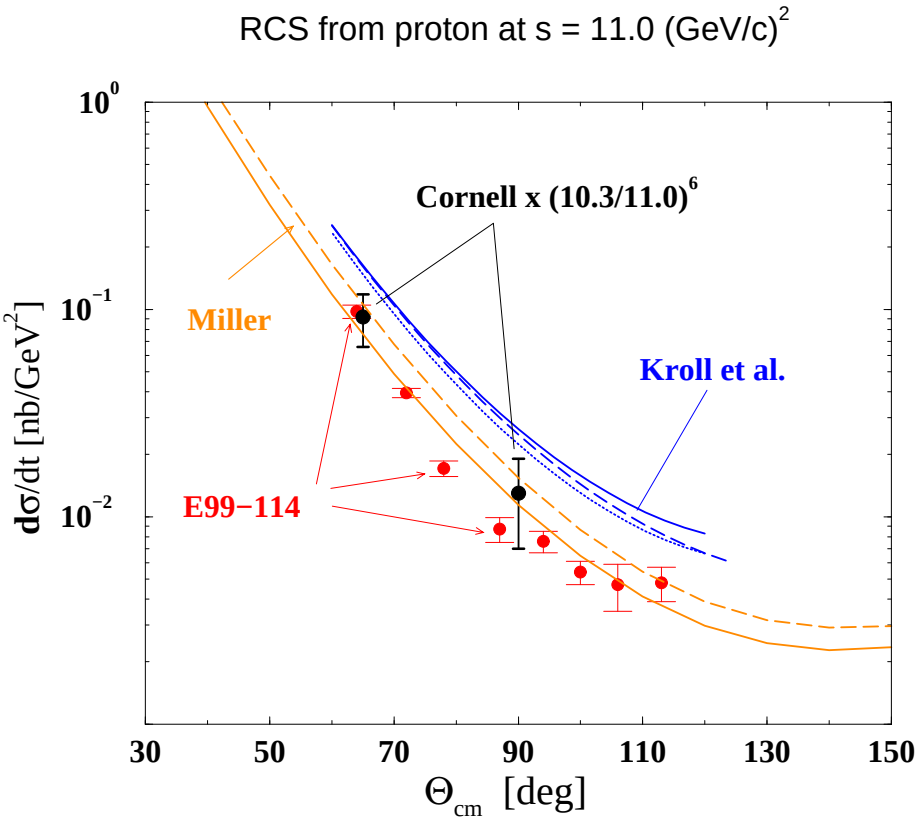

Figure 4: Cross section of RCS process at s = 11 $(\mathrm{GeV}/c)^2$ from E99-114 and Cornell[21] experiments and results of calculations in the GPD approach (Kroll) and from a CQM (Miller).

useful and intuitive picture of the hadron. The proposed test presents a unique case where predictions of the CQM and QCD–based theory are qualitatively different.

2.7 Summary of Physics Goals

We propose measurements of the spin correlation asymmetry A_{LL} at an incident photon energy of 4.3 GeV, s=9 $(\mathrm{GeV}/c)^2$, at two scattering angles; at $\theta_\gamma^{cm} = 70°$ corresponding to $-t$=2.4 $(\mathrm{GeV}/c)^2$ and at $\theta_\gamma^{cm} = 140°$ corresponding to $-t$=6.4 $(\mathrm{GeV}/c)^2$. The specific physics goals are as follows:

1. Provide a test that can expose, in an unambiguous way, how the RCS reaction proceeds: either via the interaction of photons with a current quark or, with a constituent quark.

2. Determine the form factor ratio R_A/R_V from measurement of A_{LL} and correlate these

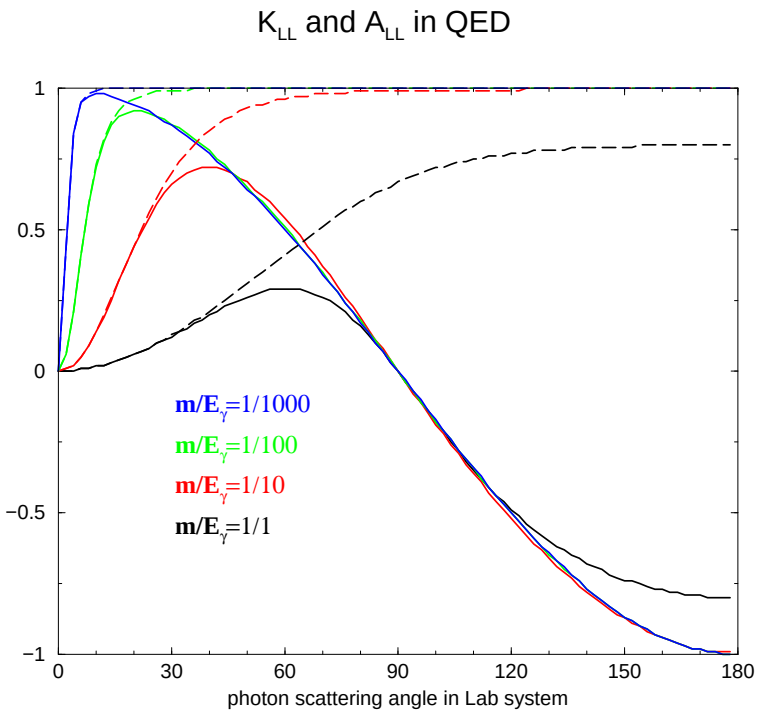

Figure 5: Klein-Nishina polarization observables A_{LL} and K_{LL} , shown by solid lines and dash lines respectively, for different ratios of the electron mass to the photon energy as a function of the scattering angle in the lab system.

measurements with the corresponding values of F_2/F_1 determined from elastic electron scattering.

The overall statistical precision with which we will address these physics goals will be discussed in Sec. 5.

3 Experimental Setup

The proposed experiment will study the scattering of polarized photons from a polarized hydrogen target, as illustrated in Fig. 6. The scattered photon will be detected in the BigCal calorimeter installed at a distance to match the acceptance of the HMS, which will be used to detect the recoiling proton.

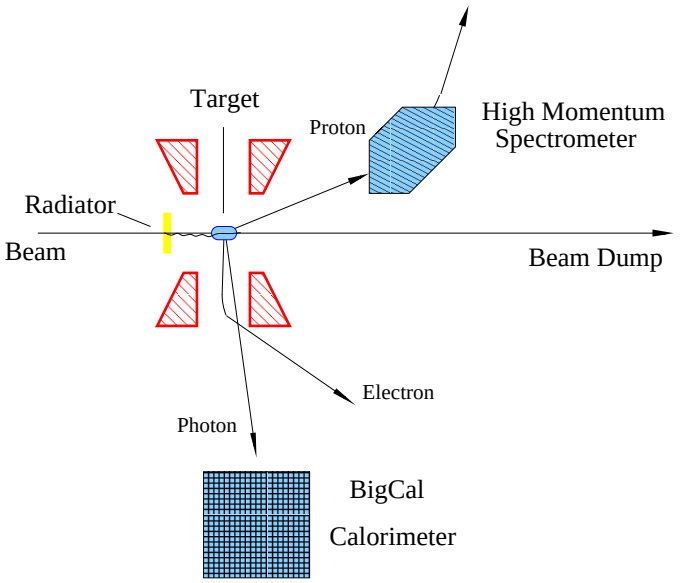

Figure 6: Schematic of the experimental setup. The target is polarized longitudinally (along the beam), scattered photons are detected in BigCal and recoil protons are detected in the HMS. Scattered electrons in the mixed photon-electron beam are deflected by the polarized target magnet.

3.1 The CEBAF Polarized Beam

We assume an incident electron beam of intensity of 90 nA and with 80% polarization. Such currents and polarizations have already been delivered using the strained GaAs source at Jefferson Lab. Such beam intensity was used on UVA polarized target with an average NH_3 polarization of 75%. The beam polarization will be measured to a systematic uncertainty of 3% with the Hall C Möller polarimeter. The large cross section and helicity asymmetry for π° photoproduction, as determined from E99-114, will provide a monitor of the electron beam polarization continuously during data taking at fixed kinematic conditions with large θ_γ^{cm}.

3.2 The Polarized Hydrogen Target and the Radiator

In this experiment we will use the U. of Virginia polarized target, which has been successfully used in E143/E155/E155x at SLAC and E93-026 and E01-006 at JLab. (See Fig. 7 for a cross section view.) This target operates on the principle of Dynamic Nuclear Polarization. The low temperature (1 K°), high magnetic field (5 T) natural polarization of solid materials (ammonia, lithium hydrides) is enhanced by microwave pumping. The polarized target assembly contains two 3–cm–long target cells that can be selected individually by remote control to be located in the uniform field region of a superconducting Helmholtz pair. The permeable target cells are immersed in a vessel filled with liquid He and maintained at 1 K by use of a high power evaporation refrigerator. The magnet coils have a 50° conical shaped aperture along the axis and a 34° wedge shaped aperture along the vertically oriented midplane.

The material, during the experiment, will be exposed to 140 GHz microwaves to drive the hyperfine transition which aligns the nucleon spins. The DNP technique produces proton polarizations of up to 95% in the NH_3 target. The heating of the target by the beam causes an initial drop of a few percent in the polarization. Then the polarization slowly decreases due to radiation damage. Most of the radiation damage is repaired by annealing the target at about 80 K, until the accumulated dose reaches $> 2 \times 10^{17}$ electrons, at which point the material needs to be changed. Due to limitations is heat removal by the refrigerator, the luminosity (considering only the polarized material in the uniform field region) is limited to 85×10^{33} cm^{-2}Hz. As part of the program to minimize the sources of systematic errors, the target polarization direction will be reversed after each anneal by adjusting the microwave frequency.

A radiator will be mounted on the liquid nitrogen shield about 10 inches upstream of the target magnet center. The short distance between the target and radiator helps to avoid background produced from Al walls of the target and downstream beam line. The separation of the events produced in the radiator is of order 5 cm in the spectrometer y coordinate, which is comfortably large compared to the y resolution of 0.3 cm. We are going to use a copper radiator with thickness of 1.43 mm (10% radiation length). Pair production in the radiator will add 9% to the heat load of the refrigerator, so that the average beam current should be reduced by 9% yielding a useful luminosity of 77×10^{33} cm^{-2} Hz. The polarized target magnet will deflect outgoing charged particles vertically, greatly simplifying the selection of the elastically scattered photons from the elastically scattered electrons at the calorimeter. The RCS experiment, E99-114, installed a magnet between the target and the calorimeter to achieve the same result, but in that case the electrons were bent in the horizontal plane. See Fig. 8.

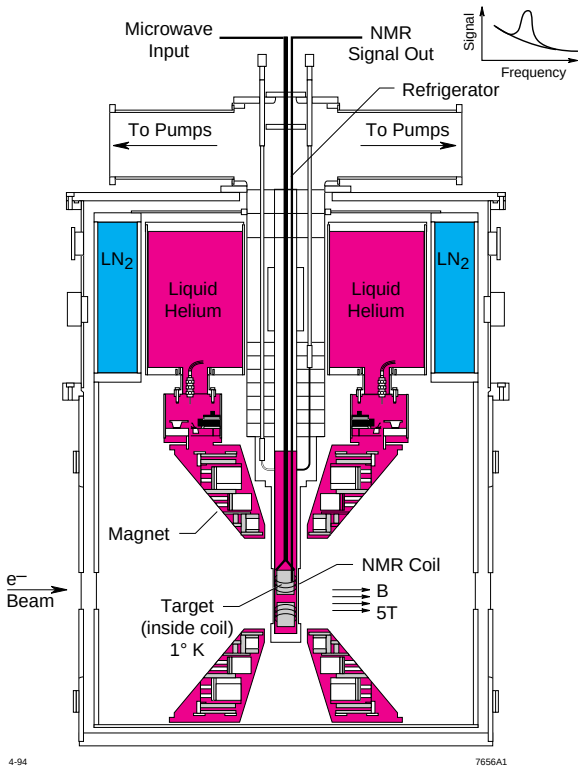

Figure 7: Cross section view of the polarized target.

3.3 The Photon Calorimeter

Members of this collaboration are participating in the construction of the BigCal calorimeter for the GEP-III experiment in Hall C [22]. This calorimeter consists of 1750 lead glass blocks of type TF-1. There are 32 columns and 56 rows of blocks. Figure 9 shows the front and top view of the calorimeter and support structure and the front end electronics.

We plan to use BigCal in two positions. The forward angle position (25° in the lab) serves two purposes: first to allow the calibration of BigCal with elastically scattered electrons and for production data taking at $\theta_{cm} = 70°$. The second position (82° in the lab) is for production running at $\theta_{cm} = 140°$. The position of the HMS, which detects the protons, will be adjusted for each kinematics to match the photon scattering angle. The distance from the target to the calorimeter is chosen to insure an adequate angular coverage of the calorimeter. As in E99-114, the movement of the calorimeter will be achieved by using the overhead crane and manual pulling of the cable train. Less than two hours (beam off to beam on) was used in a typical access into the hall for movement of the calorimeter. We will request 8 hours in the schedule for movement of the calorimeter in this experiment. Figure 9

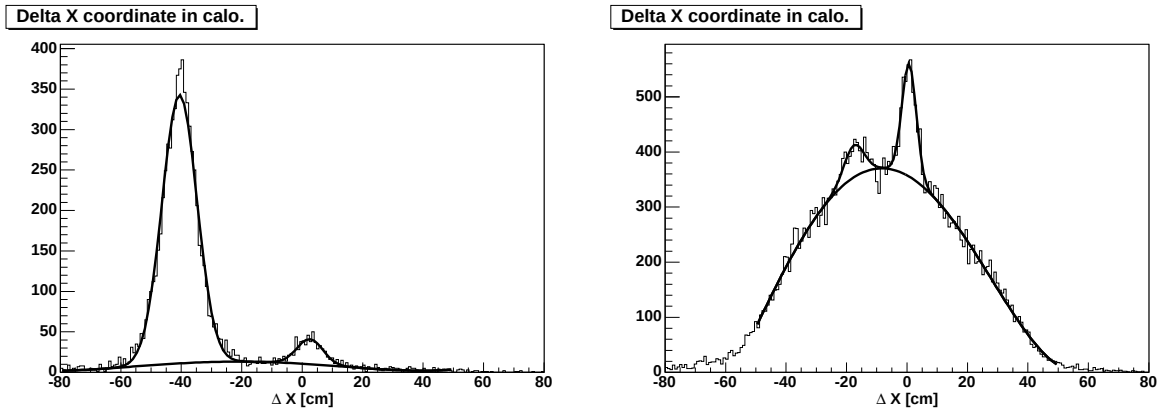

Figure 8: Experimental data from E99-114 at E = 4.3 GeV and θ_γ^{cm}=73° (left) and θ_γ^{cm}=128° (right), showing the event distribution in the correlation parameter for the horizontal plane. The peaks at coordinate $\Delta X = 0$ correspond to the RCS events. The peaks at $\Delta X = -40$ cm (left) and $\Delta X = -18$ cm (right) correspond to elastic electron scattering, shifted relative to the RCS peak by the effects of the deflection magnet.

shows the layout of the detector, the configuration of the calorimeter and the location of the front end electronics.

The energy resolution for the calorimeter, obtained at the beginning of experiment E99-114 was 5.5% (for 1 GeV photon energy) and became 10% at the end of the run as result of radiation effects on lead glass transparency. Total accumulated beam charge in the experiment E99-114 was 30 Coulomb. In BigCal the front face of the lead glass will be protected by an Al plate of 4 inch thickness to mitigate the radiation damage of the lead glass.

Members of this collaboration developed and tested, during E99-114, the technique of curing of the radiation effects in the calorimeter. This technique involves the irradiation of the glass blocks by UV light which can be done in situ without disassembling the wall. However, all the PMTs must be removed because the light intensity necessary to cure the radiation effects can damage the photocathodes. The calorimeter resolution recovery process will take about 8 shifts after GEP-III experiment is finished. Fortunately, for the measurement we propose here the total accumulated beam charge is very small, of order 0.1 Coulomb, and we can expect a very stable operation of BigCal.

3.4 Proton Polarization in the Target

Polarization of the target will be measured by NMR with an absolute accuracy on the level of 1.5%. The P1 run will provide an opportunity for the independent determination of the proton polarization. In P1 kinematics scattered electrons will be deflected in the target by 1.7 degrees in the vertical direction, which leads to displacement of 21 cm on the face

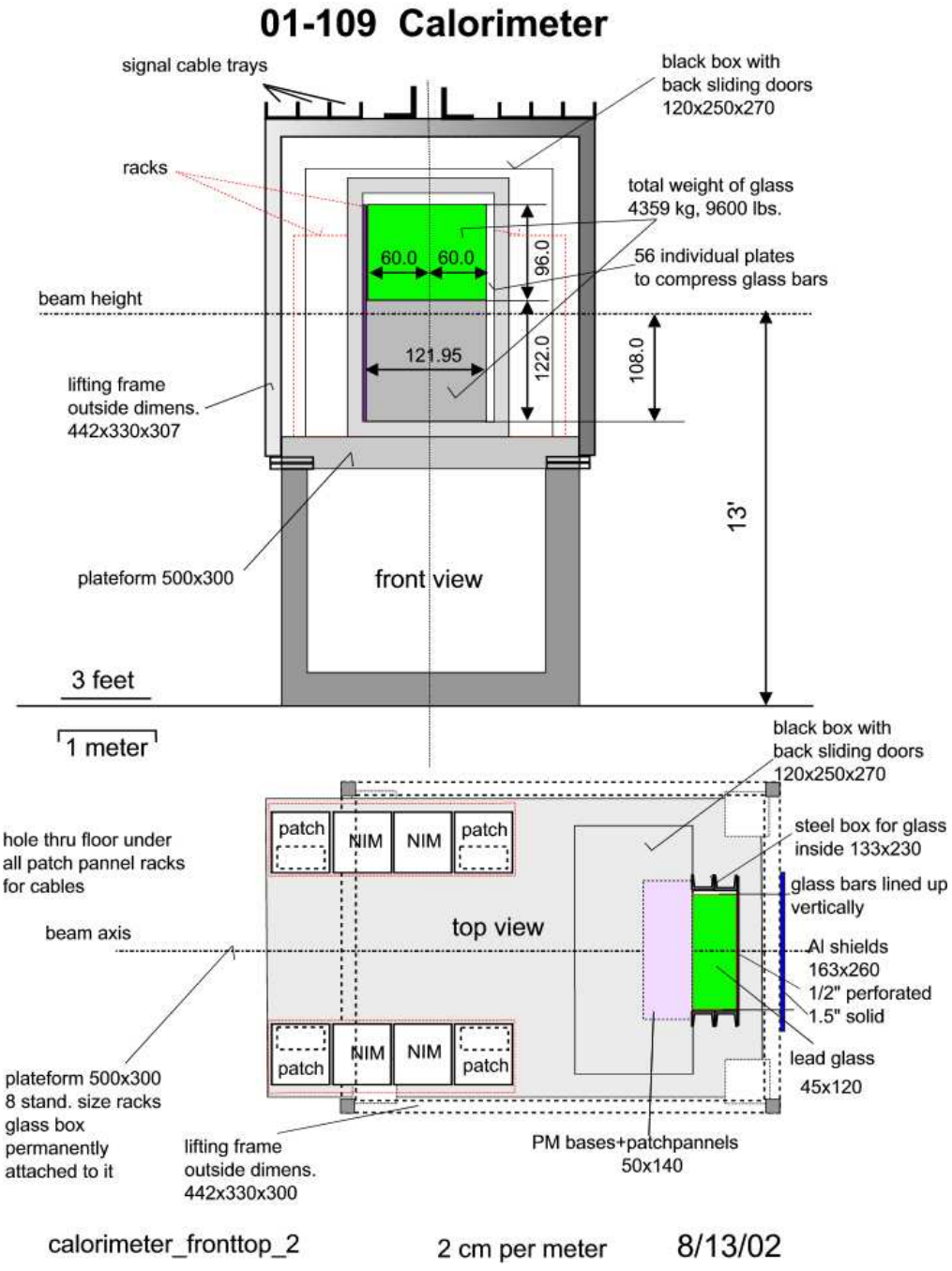

Figure 9: The structure of the BigCal calorimeter and layout of the support stand [22].

of calorimeter. For elastic electron proton scattering the beam–target asymmetry can be calculated from the following expression [23, 24]:

$$A^{ep} = \frac{2\sqrt{\tau(1+\tau)}\tan\frac{\theta}{2}}{g^2+\tau\epsilon^{-1}} \cdot (g\,\sin\phi + \sqrt{\tau}\,\cos\phi)$$

where $g = G_E^p/G_M^p$ is the ratio of the proton form factors, θ the scattering angle, $\tau = Q^2/4M_p^2$, M_p is the proton mass, and $-Q^2 = 4E_iE_f\sin^2\frac{\theta}{2}$;, $E_{i(f)}$ is the initial (final) electron energy, $\epsilon^{-1} = 1 + 2(1+\tau)\tan^2\frac{\theta}{2}$ and $\sin\phi = \cos\frac{\theta}{2}/\sqrt{(1+E_i/M_p)(2+E_i/M_p)\sin^2\frac{\theta}{2}}$. This expression explicitly takes into consideration that the polarization axis is along the beam direction and in the scattering (horizontal) plane.

For $\theta_\gamma^{cm} = 70^\circ$, $A = 0.45$. Through its measurement the product of the beam and the target polarization will be determined with a statistical accuracy of 0.02. This will provide an additional monitor of the beam and target polarization averaged over the duration of the data taking.

4 Proposed Measurements

A longitudinally polarized electron beam with current of 80 nA at energy of 4.8 GeV will be used. The Cu radiator with thickness of 1.43 mm (10% radiation length) will be installed 10 inches upstream of the 3 cm NH_3 target. Photons of average energy 90% of the electron beam energy will be used. For such bremsstrahlung photons, the circular polarization is almost equal to the polarization of the electrons. The recoil proton will be detected in the magnetic spectrometer HMS. The scattered photon will be detected in the large calorimeter BigCal.

All features of the experimental technique have been used before or our planned for use at Jefferson Lab, either in Hall C or in Hall A. Unique to this proposal is the use of a radiator in combination with the dynamically polarized target.

4.1 The Kinematics

The central momentum of the proton spectrometer will correspond to the elastic scattering of the photon (or electron) with initial energy 4.3 GeV (about 10% below the beam energy). The overlap of the acceptances of the photon and proton arms will be done the same way as in E99-114: The proton arm has the defining angular acceptance. Figure 10 shows the simulation of the incident photon spectra folded with the combined acceptances of the two arms. The effective photon energy range, defined by the acceptance overlap, is approximately 0.8 GeV.

kin. P#	t, $(\mathrm{GeV}/c)^2$	θ_γ^{lab}, degree	θ_γ^{cm}, degree	θ_p^{lab}, degree	E_γ^{lab}, GeV	p_p, GeV/c	L, m	θ_{V}^{e}, degree	θ_{V}^{p}, degree
P1	-2.4	25	70	39	3.00	2.02	7.0	1.7	4.1
P2	-6.4	82	140	12	0.87	4.25	2.5	15.4	0.6

Table 1: The kinematics parameters of the proposed measurements at $s = 9$ $(\mathrm{GeV}/c)^2$. Deflection angles θ_{V}, of the electron and the proton, show the effect of target magnetic field.

4.2 Expected Rates

In E99-114 unpolarized data were collected for the average photon energy of 4.3 GeV and θ_γ^{cm} in the range $75^\circ - 130^\circ$. Table 2 presents the cross section of the RCS process at a photon energy of 4.3 GeV. The event rates are the products of the luminosity, the cross section, and the acceptances of the detectors, as well all other factors such as DAQ dead time, efficiency of the trigger and the detectors and efficiency of the reconstruction analysis. The rate, N_{RCS} was calculated as:

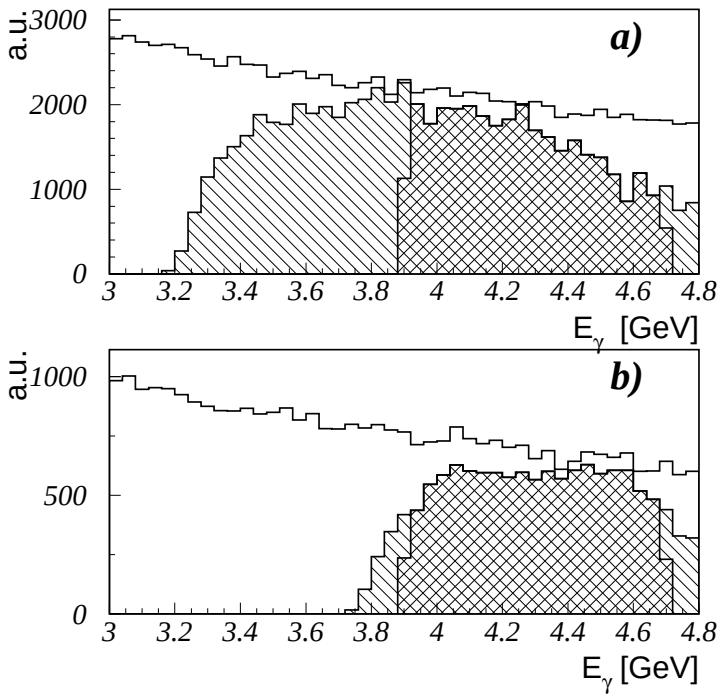

Figure 10: The simulated photon spectra for the proposed kinematics for a) for $\theta_\gamma^{cm} = 70^\circ$ and b) for $\theta_\gamma^{cm} = 140^\circ$. The photon spectra, in coincidence with the proton in the HMS, are indicated by the hashed area. The double hashed area corresponds to statistics used for our estimate of the expected results from the energy interval 3.9 – 4.7 GeV.

$$N_{RCS} = \frac{d\sigma}{dt}_{RCS} (\frac{(E_\gamma^f)^2}{\pi} \Delta\Omega_p \frac{d\Omega_\gamma}{d\Omega_p}) f_{\gamma p} (\frac{\Delta E_\gamma^f}{E_\gamma^f} \frac{t_{rad}}{X_o}) \mathcal{L}_{e\vec{p}}$$

where $\frac{d\sigma}{dt}_{RCS}$ is the RCS cross section (see Table 2); the factor $(\frac{(E_\gamma^f)^2}{\pi} \Delta\Omega_p \frac{d\Omega_\gamma}{d\Omega_p})$ is the range of Δt for the given kinematics, expressed through the energy of the scattered photon and the solid angle of the proton detector; $f_{\gamma p} = 0.5 - 0.7$ is the fraction of events detected for given range of photon energy E_γ^f; $(\frac{\Delta E_\gamma^f}{E_\gamma^f} \frac{t_{rad}}{X_o}) = 0.8/4.3 \cdot 0.128$ is the number of photons per incident electron, including the photons produced in the target and virtual photons; $\mathcal{L}_{e\vec{p}} = 7.7 \cdot 10^{34}$ cm^{-2}Hz is the electron-proton polarized luminosity with the NH_3 target, including a correction for the extra heat load from the radiator.

The simulated photon spectra for the proposed kinematics is shown in Figure 10.

Table 2 also shows the dilution factor D defined as $(N_{\gamma,\pi^\circ} + N_{\gamma,\gamma})/N_{\gamma,\gamma}$ for the kinematically correlated photon-proton events. The value of D is effected by the accuracies of the proton and the photon angles and momenta. We have used conservative estimate of D values based on E99-114 data. The cross section measured by E99-114 can be safely extrapolated

kin. 4#	θ_γ^{lab}, degree	t, $(\mathrm{GeV}/c)^2$	θ_γ^{cm}, degree	D	$d\sigma/dt$, $\mathrm{pb}/(\mathrm{GeV}/c)^2$
4A	22	-2.03	63.6	2.13	496.
4B	26	-2.57	72.8	1.54	156.
4C	30	-3.09	81.1	1.67	72.
4D	35	-3.68	90.4	2.75	42.
4E	42	-4.39	101.5	2.80	29.
4F	50	-5.04	112.1	2.42	38.
4G	57	-5.48	119.9	2.83	46.
4H	66	-5.93	128.4	3.89	61.

Table 2: The RCS cross section at s = 9 $(\mathrm{GeV}/c)^2$- 4 pass kinematics in E99-114.

to our point just outside its angular region by noting that the preliminary analysis of the data in Table 2 shows that, within ±20% systematic uncertainty, the cross section at large angles follows the expression

$$d\sigma/dt_{_{RCS}} \;=\; d\sigma/dt_{_{RCS}}|_{\theta^\gamma_{cm}=90^\circ} \cdot (1 - \cos\theta^\gamma_{cm}).$$

The distances L between the target and the calorimeter were optimized to match the acceptance of the HMS and are given in Table 1.

kin. P#	θ_γ^{lab}, degree	t, $(\mathrm{GeV}/c)^2$	θ_γ^{cm}, degree	$\frac{d\Omega_\gamma}{d\Omega_p}$	D	$N_{_{RCS}}$ per hour
P1	25	-2.4	70	0.58	1.6	11
P2	82	-6.4	140	24.5	5.5	14

Table 3: The kinematic parameters and the expected counts.

4.3 Background processes

There are several sources of physics background in this measurement. The electrons, which lose energy while passing through the radiator and the target, can scatter elastically from the protons in the target. In the RCS experiment E99-114 a deflection magnet was

used to separate the scattered electrons from the elastically scattered photons. See Fig. 8. In this experiment the field of the polarized target magnet will provide sufficient deflection. Neutral pion photoproduction from the protons in the target is another background process. It can be separated only on a statistical level by using a difference in the shapes of the distribution of RCS and H(γ, π) events shown in Fig. 8. This background leads to a large dilution factor, which effects the statistical accuracy of the measurements. The pion can also be produced from bound protons in nitrogen. Motion of the nucleons in nuclei, and FSI, reduce dramatically the dilution of RCS events. The nuclei pion process was investigated by using E99-114 data obtained from an Al target. We found that at conditions similar to those proposed here, pions produced from nuclei increase the dilution factor by less than 10%. Another background process originates in quasielastic electron scattering from nuclei in the target (He, N, etc) which will contribute a dilution on the order of 10%. These electrons will be identified by means of a lucite Cerenkov detector positioned in front of BigCal. This detector is being constructed for the SANE[25] experiment as part of BETA (Big Electron Telescope Array).

4.4 Required Statistics

The statistics required for obtaining of specified accuracy of ΔA_{LL} can be calculated from

$$N_{RCS,required} = D/(P_e P_p f_{e\gamma} \Delta A_{LL})^2$$

where $P_e = 0.80$ is the electron beam polarization, $P_p = 0.75$ is the proton polarization in the target, $f_{e\gamma} = 0.98$ is the ratio of the photon and the electron polarizations for the average $E_\gamma = 0.9E_e$. Table 4 presents required statistics for a precision of $\Delta A_{LL} = 0.05$ in kinematics P1, and $\Delta A_{LL} = 0.07$ in P2.

kinematic	P1	P2
N_{RCS}, events	1850	3250
ΔA_{LL}	0.05	0.07

Table 4: The statistics and expected precision in the proposed experiment.

5 Expected Results and Beam Time Request

5.1 Expected Results

The purpose of this experiment is to measure the initial state helicity correlation asymmetry A_{LL} with a precision sufficient to obtain conclusive evidence on the dominance of the specific reaction mechanism. Another purpose is to determine the form factor ratio: R_A/R_V, which is related to A_{LL}. We propose to obtain the statistical precision for A_{LL}, given in Table 4 and shown in Fig. 11. Using the handbag formalism to interpret the results of the A_{LL}, we will extract values for R_A/R_V.

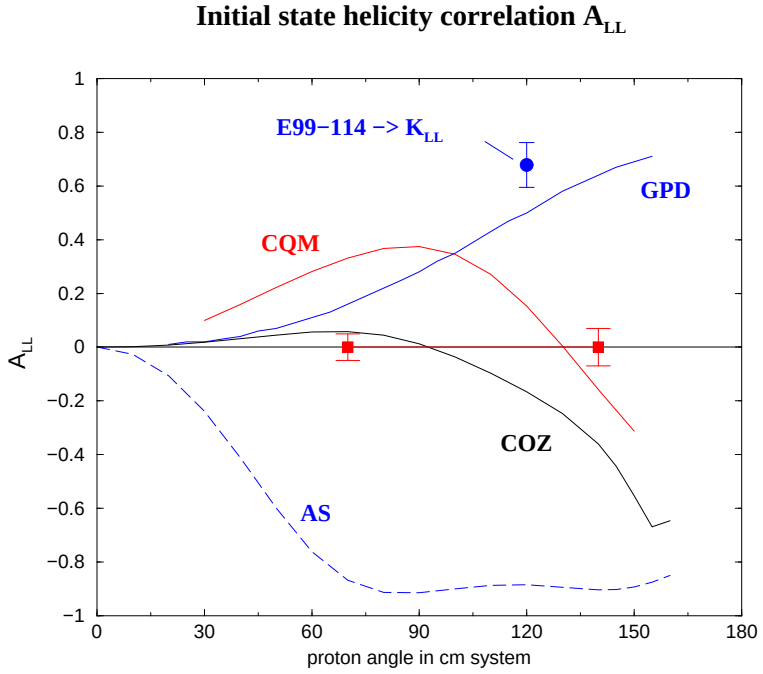

Figure 11: The initial state helicity correlation asymmetry A_{LL} in the RCS process with the expected precision of the proposed measurements shown as closed squares. The labels on the curves are as follows: CQM for the asymmetry in the constituent quark model[11]; the pQCD calculations[17] with AS for the asymptotic distribution amplitudes; with COZ for Chernyak-Ogloblin-Zhitnitsky [26]; GPD for calculations in the soft overlap approach[8]. The K_{LL} result[5] from E99-114 is also shown.

5.2 Beam Time Request

The proposed experiment will be done at one beam energy of 4.8 GeV with currents up to 1 μA. In order to achieve the results discussed above, we require the beam time summarized in Tables 5.

We require 8 hours to calibrate the calorimeter with $e + p$ elastics. To measure the packing fraction of the material in the cup, we need 16 hours to do empty cell and carbon measurements. We also request one hour per day of polarized running to measure the beam polarization with the Möller polarimeter.

Also shown in Table 5 is a summary of the time required for configuration changes. We request 3 hours per day to perform anneals of the target to restore the target polarization. We will need to change the target stick four times to load fresh material. Each of these changes will take about twelve hours to change the material and perform new target polarization calibrations. The change from P1 to P2 (move BigCal and HMS) will require 8 hours.

The total time requested is a combination of the required beam time and the overhead time. From experience running G_{En} and RSS, we know that roughly one-half of the overhead can be performed during times when the accelerator is not delivering physics beam to the Halls. Thus, our total requested time is the sum of the beam time and one-half of the overhead time. The total request is 21 days.

Kin. P#	Procedure	beam, nA	time hours
P1	BigCal calibration	1000	8
P1	RCS data taking	90	176
P2	RCS data taking	90	240
	Packing Fraction Measurements	90	16
	Moller Measurements	200	18
	Beam Time		458
	BigCal angle change		8
	Target Anneals		52
	Stick Changes		36
	Overhead Time		96
	Requested Time		506

Table 5: The beam time request for the experiment.

6 Technical Considerations

There are two experiments already approved for Hall C which will use an almost identical set up to the one proposed here. These are SANE (E03-109) and Semi-Sane (E04-113). Both experiments make use of BigCal as part of BETA (Big Electron Telescope Array) and the UVA polarized target. Additionally, Semi-SANE uses the HMS to detect hadrons. As in Semi-SANE, the longitudinal orientation of the target field in this experiment allows its operation without the chicane magnets before the target. This avoids the necessity of dumping the beam in the Hall. With proper planning the transition from one experiment to the next would not require a reconfiguration of the target or the detectors.

The radiator will be mounted on the liquid nitrogen shield of the target. It will be mounted such that it can be moved into and out of the beam as necessary so that it would not interfere with the other two experiments.

This experiment requires extensive support from the JLab. In addition to the installation of the polarized target, we will also require:

- installation of the Secondary Emission Monitor (SEM),
- beam line instrumentation workable down to 50 nA beam current,
- the large, slow raster that distributes the beam uniformly on the surface of the target,

These are fewer requirements than were necessary for the G_{En} and RSS experiment that ran from July 2001 through March 2002, so they present no special development for the laboratory.

7 Collaboration

This collaboration consists of members with extensive experience using the UVA polarized target in Hall C. In addition, the collaboration includes many individuals from the RCS collaboration in Hall A with substantial experience in electromagnetic calorimetry. We anticipate that under a similar arrangement as for G_{En} and RSS, the JLab target group together with the UVA polarized target group will handle installation, calibration and operation of the polarized target.

8 Conclusions

We request 506 hours of beamtime to measure the initial state helicity correlation asymmetry A_{LL} in RCS at s= 9 (GeV/c)^2 for $\theta_\gamma^{cm} = 70^\circ$ and 140°. This experiment will take place in Hall C, utilizing the polarized electron beam, the UVA polarized target, and HMS spectrometer to detect protons, and BigCal calorimeter to detect scattered photons. This is a unique opportunity to study the initial state polarization effects in RCS.

Knowledge of the initial state helicity correlation asymmetry A_{LL} in RCS at these kinematics will allow a rigorous test of the reaction mechanism for exclusive reactions at high t, which is crucial for the understanding of nucleon structure.

Furthermore, it will be an extended measurement of the proton axial form factor R_A in RCS, which is the $1/x$ moment of the polarized parton distribution. We propose to measure initial state helicity correlation A_{LL} at both kinematic points to a statistical precision of better than ± 0.10.

References

[1] S. J. Brodsky and G. Farrar, *Phys. Rev. Lett.* **31**, 1153 (1973).

[2] V. A. Matveev, R. M. Muradyan, and A. V. Tavkheldize, *Lett. Nuovo Cimento* **7**, 719 (1973).

[3] M. Jones *et al.*, *Phys. Rev. Lett.* **84**, 1398 (2000).

[4] O. Gayou *et al.*, *Phys. Rev. Lett.* **88**, 092301 (2002).

[5] D. J. Hamilton *et al.* [Jefferson Lab Hall A Collaboration], arXiv:nucl-ex/0410001.

[6] A.V. Radyushkin, *Phys. Rev.* **D 58**, 114008 (1998).

[7] M. Diehl, T. Feldmann, R. Jakob, P. Kroll, *Eur. Phys. J.* **C 8**, 409 (1999);

[8] H. W. Huang, P. Kroll, T. Morii, *Eur. Phys. J.* **C 23**, 301 (2002), *Erratum ibid.*, **C 31**, 279 (2003); H. W. Huang, private communication.

[9] X. Ji, *Phys. Rev.* **D 55**, 7114 (1997), *Phys. Rev. Lett.* **78**, 610 (1997).

[10] A.V. Radyushkin, *Phys. Lett.* **B 380**, 417 (1996), *Phys. Rev.* **D 56**, 5524 (1997).

[11] G. A. Miller, *Phys. Rev.* **C 69**, 052201(R) (2004).

[12] A. Nathan, and B. Wojtsekhowski, spokespersons, JLab experiment E03-003.

[13] G. P. Lepage and S. J. Brodsky, *Phys. Rev.* **D 22**, 2157 (1980).

[14] A. Radyushkin, arXive:hep-ph/0410276.

[15] G. R. Farrar and H. Zhang, *Phys. Rev. Lett.* **65**, 1721 (1990), *Phys. Rev.* **D 42**, 3348 (1990).

[16] A. S. Kronfeld and B. Nizic, *Phys. Rev.* **D 44**, 3445 (1991); M. Vanderhaeghen, P. A. M. Guichon and J. Van de Wiele, *Nucl. Phys.* **A 622**, 144c (1997).

[17] T. Brooks and L. Dixon, *Phys. Rev.* **D 62** 114021 (2000).

[18] K. Wijesooriya *et al.*, *Phys. Rev. C***66**, 034614 (2002).

[19] G. A. Miller, *Phys. Rev.* **C 66**, 032201 (2002).

[20] M. Diehl, T. Feldmann, H. W. Huang and P. Kroll, Phys. Rev. D **67**, 037502 (2003) [arXiv:hep-ph/0212138].

[21] M. A. Shupe *et al.*, *Phys. Rev.* **D 19**, 1921 (1979).

[22] C. Perdrisat *et al.*, JLab experiment E01-109, 2001.

[23] N. Dombey, Rev. Mod. Phys. 41, 236 (1969).

[24] T. W. Donnelly and A. S. Raskin, Ann. Phys. (New York) 169, 247 (1986); 191, 81 (1989).

[25] Spin Asymmetries of the Nucleon Experiment, JLAB E-03-109, O.Rondon, Z.E. Meziani, and S. Choi, spokespersons.

[26] V. L. Chernyak A. A. Oglobin, and A. R. Zhitnitsky, *Z. Phys.* **C 42**, 569 (1989).